Regulation of DNA Repair pathway choice in S/G2 by the NHEJ inhibitor CYREN

Nausica Arnoult[1], **Adriana Correia**[#1], **Jiao Ma**[#1], **Anna Merlo**[1], **Sara Garcia-Gomez**[2], **Marija Maric**[2], **Marco Tognetti**[1,3], **Christopher W. Benner**[4], **Simon J. Boulton**[2], **Alan Saghatelian**[1], and **Jan Karlseder**[1]

[1]The Salk Institute for Biological Studies, 10010 North Torrey Pines Rd., La Jolla, CA92037, USA

[2]DSB Repair Metabolism Laboratory, The Francis Crick Institute, 1 Midland Road, London NW1 1AT, UK

[4]Department of Medicine, University of California San Diego, 9500 Gilman Drive, La Jolla, CA92093, USA

[#] These authors contributed equally to this work.

Abstract

Classical non-homologous end joining 1 (cNHEJ) and homologous recombination 2 (HR) compete for the repair of double stranded breaks of DNA during the cell cycle. HR is inhibited in G1 phase of the cell cycle, but both pathways are active in S and G2 phases. Why cNHEJ does not always outcompete HR in S and G2 phases has been unclear. Here we show that CYREN is a cell cycle specific inhibitor of cNHEJ. CYREN suppression allows cNHEJ at telomeres and intrachromosomal breaks during S and G2 phases, while cells lacking CYREN accumulate chromosomal aberrations upon damage induction, specifically outside G1 phase. CYREN acts by binding to the Ku70/80 heterodimer and preferentially inhibits cNHEJ at breaks with overhangs by protecting them. We therefore propose that CYREN is a direct cell cycle inhibitor of cNHEJ, thereby promoting error free repair by HR in cell cycle phases where sister chromatids are present.

The cNHEJ machinery recognizes breaks, indiscriminately joins them and is therefore potentially genotoxic 1. HR relies on the generation of 3' overhangs, which invade homologous sister chromatids to promote error free break repair 2. Choice between HR and cNHEJ depends primarily on the cell cycle stage and the nature of the break. During G1 phase HR is inactivated, and cNHEJ is dominant, but during S and G2 phases, when sister

Correspondence should be addressed to karlseder@salk.edu.
[3]Current Address : ETH Zurich, Institute of Biochemistry, Otto-Stern-Weg 3, 8093 Zurich, Switzerland

chromatids are available, cNHEJ and HR compete 3. While the inhibition of HR during G1 is well understood, it is unclear why the abundant cNHEJ machinery does not dominate in S and G2, pointing at an active cNHEJ suppressor mechanism during and after replication. Similarly, fusions of deprotected telomeres, which occur through cNHEJ exclusively, are restricted to G1 4,5. End resection, which promotes HR, is inhibited by RIF1 and 53BP1 during G1, thereby restricting HR activity to S/G2 6–8. During S/G2, when both pathways are active 9, end-resection by CtIP is activated, which can inhibit cNHEJ 10. However, it is unclear how cNHEJ is restricted in S and G2 to allow resection and commencement of HR for error-free repair of lesions. CYREN (Cell cYcle REgulator of NHEJ) was originally identified as potential modulator of retroviral infection 11. Later, the alternatively spliced isoform CYREN-2 was found as short open reading frame translated polypeptide and to interact with the Ku70/80 heterodimer 12. We therefore tested the role of CYREN in cNHEJ and found it to be a cell cycle regulator of cNHEJ.

TRF2 is the main telomere protection factor by stabilizing the t-loop and inhibiting the ATM kinase and RNF168 13–15. Depletion of TRF2 leads to ATM activation 16 and subsequent activation of cNHEJ, leading to chromosome end-to-end fusions 17, while HR and alternative NHEJ (altNHEJ) remain inhibited by shelterin and Ku70/80 18–20. Chromosome fusions prior to replication occur between the single chromatids of two chromosomes, leading to chromosome-type fusions after replication, where both sister chromatids are fused. When fusions occur after replication, only one sister chromatid is engaged in the fusion, leading to chromatid-type fusions (Figure 1a). Chromosomes fused as a result of TRF2 loss display as chromosome-type fusions during metaphase, demonstrating that the fusion process is restricted to G1 of the cell cycle and suppressed during S and G2 4,5,21,22. The emergence of chromatid type fusion signifies a derepression of cNHEJ in S and G2 (Figure 1a), representing a powerful system to investigate DSB repair pathway choice. To study the role of CYREN in cNHEJ, we generated HT1080 6TG cells with three stably integrated inducible shRNAs targeting CYREN (shCYREN#A,B,C), which were induced after TRF2 depletion followed by metaphase analysis (Extended data Figure 1a-c, Extended data Figure 10). Depletion of TRF2 alone led to chromosome type G1 fusions, while chromatid-type fusions were rare (Figure 1b-c, Extended data Figure 1d-e). Overall chromosome-type telomere fusion frequency was unaltered by CYREN depletion (Figure 1c, Extended data Figure 1d-e, g), indicating that CYREN is not part of the cNHEJ machinery. Instead, depletion of CYREN and TRF2 led to a five-fold increase in chromatid-type fusions (Figure 1b-c, Extended data Figure 1d-e, g), suggesting that CYREN could suppress cNHEJ in S and G2 at deprotected telomeres. Sister telomere associations were not increased (Extended data Figure 1f-g) and cell cycle dynamics were not perturbed by shRNA treatment (Figure 1d). Untransformed IMR90+E6E7 fibroblasts reacted comparably (Extended data Figure 2a-d). CYREN depletion did not lead to chromatid-type fusions at intact telomeres, indicating that CYREN itself does not play a role in end protection (Figure 1b-c, Extended data Figure 2d-e).

Chromosome-Oriented FISH on CYREN and TRF2 co-depleted cells found no bias in the type of chromatid involved in the chromatid-type fusions, ruling out that the observed fusions are a result of unprocessed leading strand overhangs 23,24 (Extended data Figure 3a-b). To determine whether the fusions were the result of cNHEJ or altNHEJ activation, we

depleted ATM, Ligase 4, DNA-PKcs and Ligase 3 in TRF2-suppressed CYREN wild type and knockout cells (Extended data Figure 3c-d). Only ATM, Ligase 4 or DNA-PKcs depletion suppressed both chromosome- and chromatid-type fusions, indicating that CYREN regulates cNHEJ, not altNHEJ (Figure 1e). ATM, DNA-PKcs or PARP inhibitors 25–27 yielded comparable results, while inhibition of RAD51 28 had no effect, excluding that CYREN controls HR (Extended data Figure 3e-f). ATM and DNA-PKcs inhibition for 48 hours suppressed both chromosome- and chromatid-type fusions, but only the chromatid-type fusions were suppressed when inhibition occurred during S and G2 phases, while inhibition during G2 had an intermediate effect (Figure 1f), confirming that CYREN inhibits cNHEJ in S and G2 phase at deprotected telomeres.

To demonstrate that CYREN is a genome-wide regulator of DSB repair pathway choice, we first tested the effects of CYREN deletion on the repair of irradiation-induced intrachromosomal breaks. While three synchronized CYREN^{wt} and CYREN^{KO} clones (Extended data Figure 10) accumulated rearrangements or bridges after irradiation in G1, cells lacking CYREN amassed significantly more abnormalities when irradiated during and after replication (Figure 2 a-b, Extended data Figure 4 a-b), pointing at a role of CYREN at intrachromosomal breaks in S and G2. We then designed an *in vivo* fluorescence-based reporter system that allows the quantitative comparison of cNHEJ and alt-NHEJ versus HR in the same cells through the repair of two inverted ISce1 cuts. Repair through NHEJ or HR leads to GFP or mCherry expression, respectively, while transfection efficiency was controlled using BFP expression from the repair donor cassette (Figure 2c, Extended data Figure 4c-d, Extended data Figure 10). We confirmed that all isolated reporter clones (Extended data Figure 4e) followed the same cell cycle kinetics (Extended data Figure 4e) and analysed the outcome of repair by flow cytometry. The CYREN knockout clones utilized NHEJ significantly more frequently than the wild type clones, while HR was significantly reduced in the same cells (Figure 2d). CYREN depletion did not lead to the formation of radial chromosomes, or to an increase in radials in cells lacking *Brca1*, or a decrease in survival (Extended data Figure 5a-c), arguing against the role of CYREN in replication-induced DSB repair pathway, where HR is dominant.

As a result of alternative splicing of *C7orf49,* three isoforms of CYREN are generated (Figure 3a), of which isoforms 1 and 2 were found to bind to Ku70/80 12. We expressed the Flag-tagged isoforms, depleted TRF2 and suppressed endogenous CYREN by targeting the 3' UTR of C7orf49 (Extended data Figure 6a-b). 3' UTR siCYREN increased chromatid-type fusions in control cells or cells expressing CYREN-3, but CYREN-1 or CYREN-2 rescued the phenotype (Figure 3b), indicating that they inhibit cNHEJ.

To verify the endogenous expression levels of the isoforms we inserted a 3xFLAG tag at the N-terminus of CYREN-1 and 2 and the C-terminus of CYREN 1 and 3 (Extended data Figure 6c-h, Extended data Figure 10). CYREN-1 was six to seven times more abundant than CYREN-2 (Extended data Figure 6e), CYREN-3 expression was not detectable (Extended data Figure 6h) and the siCYREN approach indeed targeted endogenous CYREN (Extended data Figure 6i). We therefore focused on CYREN-1.

To identify the CYREN-1-Ku interaction domain, we incubated a CYREN-1 peptide array with recombinant Ku70/80 (Extended data Figure 7a). Ku70/80 bound to several peptides on the N-terminus of CYREN-1, a region that is lacking in isoform 3. Alanine mutagenesis, followed by co-immunoprecipitation of Ku70/80 with mutated CYREN-1, identified R11, P14 and W16 as the precise interaction domain (Figure 3c, Extended data Figure 7b). These highly conserved residues (Extended data Figure 7c) are part of the Ku-binding motif (KBM), previously also described in APLF, CYREN and WRN and shown to interact with a hydrophobic pocket in the vWA domain of Ku80 29. We incubated a synthetic UV-crosslinkable BPA-BIO-CYREN peptide with cell lysate, followed by UV crosslinking and biotin pulldown, and confirmed the direct CYREN KBM-Ku80 interaction (Extended data Figure 7d).

Co-depletion of CYREN and TRF2 again led to chromatid-type fusions, which were suppressed by exogenous expression of wild type CYREN-1 as well as CYREN-1^{R11A} (Extended data Figure 7e, Figure 3d). In contrast, expression of the CYREN-1^{P14A} and CYREN-1^{W16A} mutants, as well as the triple mutant CYREN-1$^{RPW-AAA}$, failed to rescue the chromatid-type fusions (Figure 3d), indicating that the CYREN mediated inhibition of cNHEJ critically depends on the interaction of CYREN with Ku.

Because CYREN activity is strictly restricted to S and G2, we examined the cell cycle regulation of CYREN. CYREN-1 and CYREN-2 mRNA levels, endogenous C-terminally tagged CYREN-1 or endogenous N-terminally tagged CYREN-1 and CYREN-2 proteins were not cell cycle regulated (Figure 3e-f, Extended data Figure 7f). In contrast, the interaction of CYREN with the Ku heterodimer was restricted to S and G2 of the cell cycle (Figure 3g-h), explaining the cell cycle dependency of CYREN based c-NHEJ inhibition.

To understand whether CYREN has a preference for break sites with pre-existing overhangs, we generated breaks that either bear blunt ends or 5' or 3' overhangs of different lengths at an m-Clover-LaminA reporter (Figure 4a, Extended data Figure 10). We found that although CYREN depletion did not affect the repair of blunt ends, HR was reduced at breaks with overhangs (Figure 4b, Extended data Figure 8a). The reduction reached up to 40% at breaks with long 3' overhangs, suggesting that CYREN preferentially regulates cNHEJ at breaks with overhangs, consistent with the strong cNHEJ inhibition observed at telomeres. To analyse a potential role for CYREN in overhang processing during cNHEJ, we used the same reporter system without providing a HR donor. Deep sequencing and analysing the deletions at the repair junctions revealed no increased deletion frequencies at blunt ends, but the lack of CYREN led to increased deletions of the 5' and 3' overhangs, indicating that CYREN prevents the processing of overhangs (Figure 4c, Extended data Figure 8b). This phenotype was rescued by CYREN^{wt} expression, but not by CYREN mutant that fails to interact with Ku70/80 (Extended data Figure 8c-d). The data suggest that CYREN protects the single stranded overhangs at break sites, thereby creating a local environment that favours HR, while preventing cNHEJ dependent repair.

CYREN had previously been described as stimulator of end joining in vitro 12. However, when we compared in vitro NHEJ activities of CYREN knockout with wild type clones, we did not observe differences (Extended data Figure 9a). Similarly, purified wild type CYREN

or CYREN incapable of binding to Ku did not stimulate end joining activity (Extended data Figure 9b), leading us to the conclusion that the small differences reported previously were likely the consequences of oversaturating the reaction with recombinant protein.

CYREN represents a novel class of pathway choice regulators that is not a functional part of the cNHEJ or HR machineries *per se*. Possibly the CYREN-Ku interaction diminishes binding of Ku to break sites with overhangs. Similarly, CYREN could compete for Ku binding with other KBM containing factors in vivo, thereby obstructing initiation of the NHEJ process and giving the resection machinery an advantage, consistent with the observation that HR is favoured when rapid end joining by NHEJ is inhibited 30. While inhibition of HR at replication-induced breaks eventually leads to repair by cNHEJ even in S and G2, cNHEJ at telomeres remains inhibited, possibly because the overhangs of two deprotected telomeres are not cohesive and fusion depends on overhang processing, which does not apply to the cohesive overhangs induced by nickase. CYREN could therefore suppress the fusion of distal breaks bearing overhangs and prevent translocations in S and G2. Finally, understanding CYREN will permit an in-depth analysis of the cell cycle regulated Ku-CYREN interaction and the potential effects on toxicity of error prone repair, whether unleashing cNHEJ in cell cycle phases other than G1 will predispose organisms to cancer and whether deregulation of cNHEJ in S and G2 sensitizes cancer cells to genotoxic drugs.

Methods

Cell culture

HT1080, HT1080 6TG (ATCC) and their derivatives cells were grown in Glutamax-DMEM supplemented with 0.1 mM nonessential amino acids and 10% bovine growth serum. Human IMR-90 primary lung fibroblasts transformed with E6E7 1 were grown in Glutamax-DMEM (Gibco) supplemented with 0.1 mM nonessential amino acids and 15% fetal bovine serum. All cells were grown at 7.5% CO_2 and 3% O_2. All cell lines were purchased from ATCC or have been commercially authenticated and tested free of mycoplasma. When indicated, cells were treated with the following inhibitors: ATMi (KU-55933, Tocris, 10μM), DNA-PKcsi (NU-7441, Tocris, 1μM), PARPi (Olaparib, Selleck Chemical, 10μM), RAD51i (RI-1, Selleck Chemical, 20μM).

Plasmids, transfections and infections

TRF2 shRNA in pLKO.1 was obtained from Open biosystems. The non-coding control shRNA in pLKO.1 was obtained from David Sabatini via Addgene (Plasmid 1864, 2). Inducible Luciferase control and CYREN shRNAs in a pRSITUR plasmid were obtained from Cellecta, target sequences are listed bellow. CYREN-1-Flag, CYREN-2-Flag and CYREN-3-Flag were cloned in pCDNA3 plasmid. Inducible CYREN-1-3xFlag and its mutant derivatives were cloned in pLIX lentiviral inducible expression vector, obtained from David Root via Addgene (Plasmid 41395). Small guide RNAs targeting CYREN (target sequences detailed bellow) were cloned in pX330 plasmid obtained from Feng Zhang via Addgene (Plasmid 42230, 3). pCBASce1 plasmid was obtained from Maria Jasin via Addgene (Plasmid 26477, 4). DSB reporter system plasmid (pDRR), mCherry HR donor

plasmid (pDonor HR mCherry), 3FLAG-C7orf49 donor plasmid (pDonor 3FLAG C7Orf49), mClover-LMNA donor plasmid (pDonor mClover-LMNA) and LMNA Nickase Reporter plasmids (pCas9D10A-sgLMNA) were obtained by DNA synthesis of gBlocks (IDT DNA) and cloning by InFusion (Clontech). pDRR was cloned in a pLenti CMV Neo backbone obtained from Eric Campeau via Addgene (Plasmid 17447, 5). pDonor HR mCherry, pDonor 3FLAG C7Orf49, pDonor C7Orf49 3FLAG and pDonor mClover LMNA were cloned in pCBA backbone (Addgene plasmid 26477). pCas9D10A-sgLMNA plasmids were cloned in pX460 backbone obtained from Feng Zang via Addgene (Plasmid 48873, 3). All plasmid maps are depicted in Extended data Figures 10-11.

Transient transfections were performed using either Nucleofection (Lonza) or Lipofectamine3000 (Thermo Fisher), following manufacturer's instructions.

Lentivirus was produced by the Salk's Gene Transfer, Targeting and Therapeutics Core facility or in the laboratory. For virus production, 293FT cells (Thermo Fisher) were transfected with 7μg of plasmid using Lenti-X Packaging Single-shot system (Clontech). Viral supernatant was collected 48 hours after transfection and used for cell infection at a multiplicity of infection (MOI) of 2 in the presence of LentiBlast (Oz biosciences). 48 hr after infection, cells were washed and selected with 1 μg ml^{-1} puromycin for two days, 800 μg ml^{-1} G418 (neomycin^R) for 10 days or 75 μg ml^{-1} Hygromycin B for 10 days. pRSITUR infected cells were sorted for RFP fluorescence.

List of siRNAs, sgRNAs, shRNAs and primers used

shRNAs plasmids and target sequences:

shTRF2	pLKO.1 (Open Biosystems)	ACAGAAGCAGTGGTCGAATC
shLuci	pRSITUR (Cellecta)	CGCTGAGTACTTCGAAATGTC
shCYREN-A	pRSITUR (Cellecta)	CTCTGGGAATCCTGATTGAGA
shCYREN-B	pRSITUR (Cellecta)	GAAGAGGATGTGCTGAAATAC
shCYREN-C	pRSITUR (Cellecta)	GGATGTGCTGAAATACGTCGC

sgRNAs target sequences:

CYREN KO and N-ter tagging: AAGGACCCTCGTTTTAGTCT. CYREN C-ter tagging: GGCCGCCCGCCTGTGGGAAT. Cas9 reporter, Blunt ends: GGTTGGCAGCGCTGCCCGCG. 44bp 5' overhangs (Cas9D10A) or 3' overhangs (Cas9N368A): GGTTGGCAGCGCTGCCCGCG & CCATGGAGACCCCGTCCCAG. 96bp 5' overhangs: CGCTGCCAACCTGCCGGCCA & TGCTCGGAGTCGGAGTGCGC. 37bp 3' overhangs: CCCGAGCCCCGCGCCCTTTC & ACGGGGTCTCCATGGCCGGC. 94bp 3' overhangs: CAAGCCGAGAGCCAGCCGGC & ACGGGGTCTCCATGGCCGGC

siRNA sequences:

Non-targeting pool (NT): UGGUUUACAUGUCGACUAA, UGGUUUACAUGUUGUGUGA, UGGUUUACAUGUUUUCUGA, UGGUUUACAUGUUUUCCUA.

CYREN 3' UTR: CCUAGAAAGCAAACGAGCU, GCAGCUAGCUAUAAAGCAA, AUACACAAGUGCUAGAAAA.

ATM: GCAAAGCCCUAGUAACAUA, GGUGUGAUCUUCAGUAUAU, GAGAGGAGACAGCUUGUUA, GAUGGGAGGCCUAGGAUUU.

Ligase 4: GCACAAAGAUGGAGAUGUA, GGGAGUGUCUCAUGUAAUA, GGUAUGAGAUUCUUAGUAG, GAAGAGGGAAUUAUGGUAA.

DNA-PKcs: GGAAGAAGCUCAUUUGAUU, GAGCAUCACUUGCCUUUAA, GCAGGACCGUGCAAGGUUA, AGAUAGAGCUGCUAAAUGU.

Ligase 3: GGACUUGGCUGACAUGAUA, GACAUUGCCUCCAGGUGUA, CAGAAGUGGUGCACAGUCA, GAAGGGCGUAUGCCGAAUU.

Primers for PCR and RT-PCR:

CYREN-1: GTCCTTCCCTCATGGCTGAC & TCCTTGTCGCAGGGAGTCTT.

CYREN-2: ACTCCTGCGAATCTGACTC & AATCAGGATTCCCAGAGCA.

CYREN-3: TTGTGAGAAGACTCCCTGC & AATCAGGATTCCCAGAGCA.

ACTB: TGTACGCCAACACAGTGCTG & GCTGGAAGGTGGACAGCGA.

LMNA reporter: TACACCAGCCAACCCAGATCC & CGATCATTGAGCTCCTGCAGG

Telomere FISH and CO-FISH

For fusions analysis, cells were synchronized in metaphase with 20 ng ml^{-1} colcemid for 30 min (Figure 2D) or 3 hr, collected by trypsinization and centrifuged. Hypothonic choc was performed 7 min at 37ºC in 75mM KCl, followed by fixation in Methanol:Acetic acid 3:1 (v/v). After three washes in fixative solution, cells were dropped on superfrost microscope slides and dried over night. Slides were then rehydrated 10 min in PBS, fixed 2 min in 3.7% (v/v) formaldehyde in PBS and dehydrated in ethanol bath series (70%; 90%; 100%, 3 min each) and air dried. Slides were layered with 40μl of 0.3ng μl^{-1} Alexa488-OO-(CCCTAA)$_3$ PNA probe (PNA Bio Inc.) diluted in 70% (v/v) deionized formamide; 0.25% (v/v) blocking Reagent (NEN); 10mM Tris pH 7.5; 4.1mM Na$_2$HPO$_4$; 450μM citric acid; 1.25mM MgCl$_2$, denatured 4 min at 76ºC and incubated 2 hr at room temperature. Slides were then washed twice 15 min 70% (v/v) formamide; 10mM TrisHCl pH 7.5 and three times 5 min in 50mM TrisHCl pH 7.5; 150mM NaCl; 0.08% Tween-20. Slides were stained with 50ng ml^{-1} DAPI, dehydrated in ethanol bath series, air-dried and mounted in Prolong-Gold (Thermo Fisher).

CO-FISH was performed as described 6.

Immunoblotting

Immunoblotting was performed as described 7 and developed using a Syngene G-Box imager. Antibodies: TRF2 (Karlseder lab), Rabbit FLAG (Sigma-Aldrich - F7425), FLAG (M2, Sigma-Aldrich - F1804), Tubulin (Sigma-Aldrich – T6557), BrdU A488 (3D4, BD Biosciences - 555627), Ku70 (V540, Cell Signalling - 4104), Ku70 (Abcam – ab3114), Ku86 (Cell Signalling - 2753), ATM (Epitomics - 1549-1), Ligase 4 (EPR16531, Abcam - ab193353), DNA-PKcs (Abcam - ab70250), Ligase 3 (BD Biosciences - 611876), Anti-Rabbit HRP (GE Healthcare - NXA931), Anti-Mouse HRP (GE Healthcare - NXA934V).

Peptide binding assay

Peptide binding arrays were generated as previously described 8. Membranes were activated by soaking 2 min in methanol, washed 5 min in TBST, blocked 5 min in TBST + 5% milk (TBST-M), and incubated 24 hr at 4ºC with 6 μg ml^{-1} of purified Ku70/Ku80 proteins in TBST-M, followed by incubation overnight in anti-Ku70 primary antibody diluted 1:1000 (v/v) in TBST-M. Membranes were then washed three times 5 min in TBST, incubated 1 hr with secondary antibody, washed three times 15 min in TBST, revealed with ECL substrate and imaged with a Syngene G-Box imager.

Co-Immunoprecipitations

For Alanine scan, CYREN1-FLAG was cloned in pcDNA3.1 construct and residues 9 to 46 were each mutated to an Alanine using Q5 Site-Directed Mutagenesis Kit (NEB). HEK293T cells were transfected with 10μl of empty vector, FLAG-tagged CYREN1 wt or mutants using Lipofectamine 2000. 24 hours post-transfection, cells were harvested and lysed with Pierce IP lysis buffer (Thermo Fisher) supplemented with protease inhibitors (Roche). Protein lysates were immunoprecipitated with anti-FLAG agarose beads (clone M2, Sigma Aldrich) 1 hr at 4°C for, washed 3 times with TBS-T and eluted with 125 μg ml^{-1} 3X FLAG peptide (Sigma Aldrich) in TBS-T 1 hr at 4°C. 2.5% of the cell total lysate and 25% of the immunoprecipitate were used for western blot analysis.

For endogenous CYREN immunoprecipitations, cells were synchronized by double thymidine block and lysed in Pierce Lysis buffer 30 minutes after 2 Gy irradiation in S, G2 or G1 (respectively 4, 9 and 12.5 hours after Thymidine release). 500μg of protein lysates were incubated overnight with 2μg of rabbit anti-Flag or control IgG antibody followed by one hour incubation with 50μl of Dynabeads Protein G. Beads were washed five times in PBST and boiled in Laemli buffer. 2.5% of the cell total lysate and 25% of the immunoprecipitate were used for western blot analysis.

Photo-crosslink pulldown

Purified CYREN(2-24) free peptide and cross-linkable CYREN(2-24)- (p-benzoyl-l-phenylalanine (BPA at residue 16)-Biotin peptides were purchased from RS synthesis. 2 mg of HEK293T cell lysates were incubated 1 hr at 4ºC 100μM CYREN(2-24) free peptide (or equivalent volume of DMSO). 25-50μM CYREN(2-24)-BPA(16)-Biotin were added and incubation was pursued 2 hr, followed by UV crosslinking (Stratalinker 1800, 365nm) for one hour while maintaining samples on ice. Crosslinked samples were immunoprecipitated 1 hr at 4ºC with 100 μL of streptavidin agarose beads (Thermo FISHER), washed 3 times with

TBS-T supplemented with 1% SDS at room temperature for three times, 15 min each. The samples were eluted with 2X SDS loading dye and boiled for 15 min at 95 °C. SDS-PAGE and Western blot analysis were performed.

In Vitro End-Joining Assay

Cells were wash three times in ice-cold PBS, resuspended in two volume of hypotonic lysis buffer (10 mM Tris-HCl, pH 8.0/ 1 mM EDTA/ 1 mM DTT plus protease inhibitors), left 20 minutes on ice. Swollen cells were lysed by homogenization left 20 min on ice, and 0.5 volume of high salt buffer (50 mMTris-HCl, pH 7.5/ 1MKCl/ 2mMEDTA/ 1mM DTT) was added. Extract was centrifuged for 1 hour at 20,000 rpm in a Beckman 70.1 Ti fixed angle rotor 4°C, using polycarbonate thick wall tubes. Supernatant was dialyzed for 2-3 hours against E buffer [20 mM Tris-HCl, pH 8.0/ 0.1 M KOAc/ 20% (vol/vol) glycerol/ 0.5 mM EDTA/ 1 mM DTT] in a cassette with a membrane cutoff of 10000 Da. Snap freezing in liquid N2 and storage at -80° C. End-Joining reactions (20 μl) were carried out in 20 mM Tris-HCl (pH 7.5), 01 mM Mg(OAc)$_2$, 60 mM KOAc, 2 mM ATP, 0.5 mM DTT, and 80 μg/ml BSA, 40 ng of cell extracts and 20 ng of 32P-labeled DNA. Incubation was for 90 minutes at 37°C. 32P-labeledDNAproducts were deproteinized and analyzed by electrophoresis through 0.6% agarose gels followed by autoradiography. Quantification of joining efficiency was carried out using ImageJ. Linear DNA containing 3'-overhangs was generated by cutting the plasmid pBLueScript with the endonuclease HindIII, 5'-overhangs were generated cutting with KpnI and blunt ends were generating using EcoRV.

DSB Repair Reporter (DRR)

The integrated DRR consists of a promoter and resistance cassette fused to a T2A peptide and two inverted ISce1 sites, followed by GFP. Intact or partially cut DRR lack GFP expression due to the presence of a STOP codon. Cells are transfected with ISce1 and an exogenous donor for HR. Repair by NHEJ or HR lead to GFP or mCherry expression.

Protein alignment

We used PRALINE protein alignment online software. http://www.ibi.vu.nl/programs/pralinewww/

Flow Cytometry

For DNA repair reporter analysis, one million cells containing integrated reporter were nucleofected with 4μg of pDonor HR plasmid and 2.5μg of pCBASce plasmid. 48 hr after transfection, cells were trypsinized and resuspended in 25mM HEPES pH 7; 1% (v/v) FBS; 2mM EDTA; 1x PBS and directly subjected to flow cytometry analysis. For Cas9-LMNA reporter, 0.4 million cells were seeded in a 6-well plate and transfected 24 hours later using Lipofectamine 3000 with 4μg of mClover-LMNA HR donor plasmid and 2.5 μg of a plasmid expressing Cas9 D10A and a pair of gRNAs. Cells were analyzed by flow cytometry 72 hours after transfection. For cell cycle analysis, cultured cells were treated 10 min with 30 μM BrdU, fixed in PBS:Ethanol 1:3 (v/v) and labeled with Alexa488 anti BrdU and Propidium Iodide. Flow cytometry was performed using MACSquant Analyzer 10 (Miltenyi) and analyzed with FlowJo10.

Deep Sequencing

CYRENwt and KO clones were transfected as for flow cytometry analysis, except no HR donor was transfected. Four days after transfection, DNA was extracted using Quick-DNA Miniprep Plus kit (Zymo Research) and a 300nt region around the break sites was amplified by PCR using KOD hot start polymerase (Millipore). Transfection efficiency was controlled by flow cytometry with the BFP tag on the Cas9 guide RNA plasmid. PCR products were sequenced by MiSeq by Retrogen. The paired end fastq files were first merged into single continuous reads using FLASH (PMID:21903629). Reads were then aligned to the amplified template reference sequence of the amplified template using global Smith-Waterman sequence alignment with the EMBOSS Needle program using default parameters (PMID: 10827456). Only sequences with an alignment score of at least 800 were considered Deletions were compiled from the alignments of correctly aligning sequences.

Statistical Analysis

Each figure legend indicates sample size and number of independent experiments. ****$P<0.0001$, ***, $P<0.001$, **$P<0.01$, *$P<0.05$, ns non significant. To detect trends among multiple data sets in Fig. 1c-f, Fig. 3b-h, Fig. 4b and Extended data Fig. 2d, one-way ANOVA was used. Percentage of cells with fusions in Fig. 1e, Fig. 3d and Extended data Fig. 1e and 3f were analysed by Fisher's exact test. Two tailed unpaired t test was used in Fig. 2a-b-d and Extended data Fig. 8c to compare two data sets where Gaussian distribution is assumed. All statistical analyses were performed using GraphPad Prism 7 software.
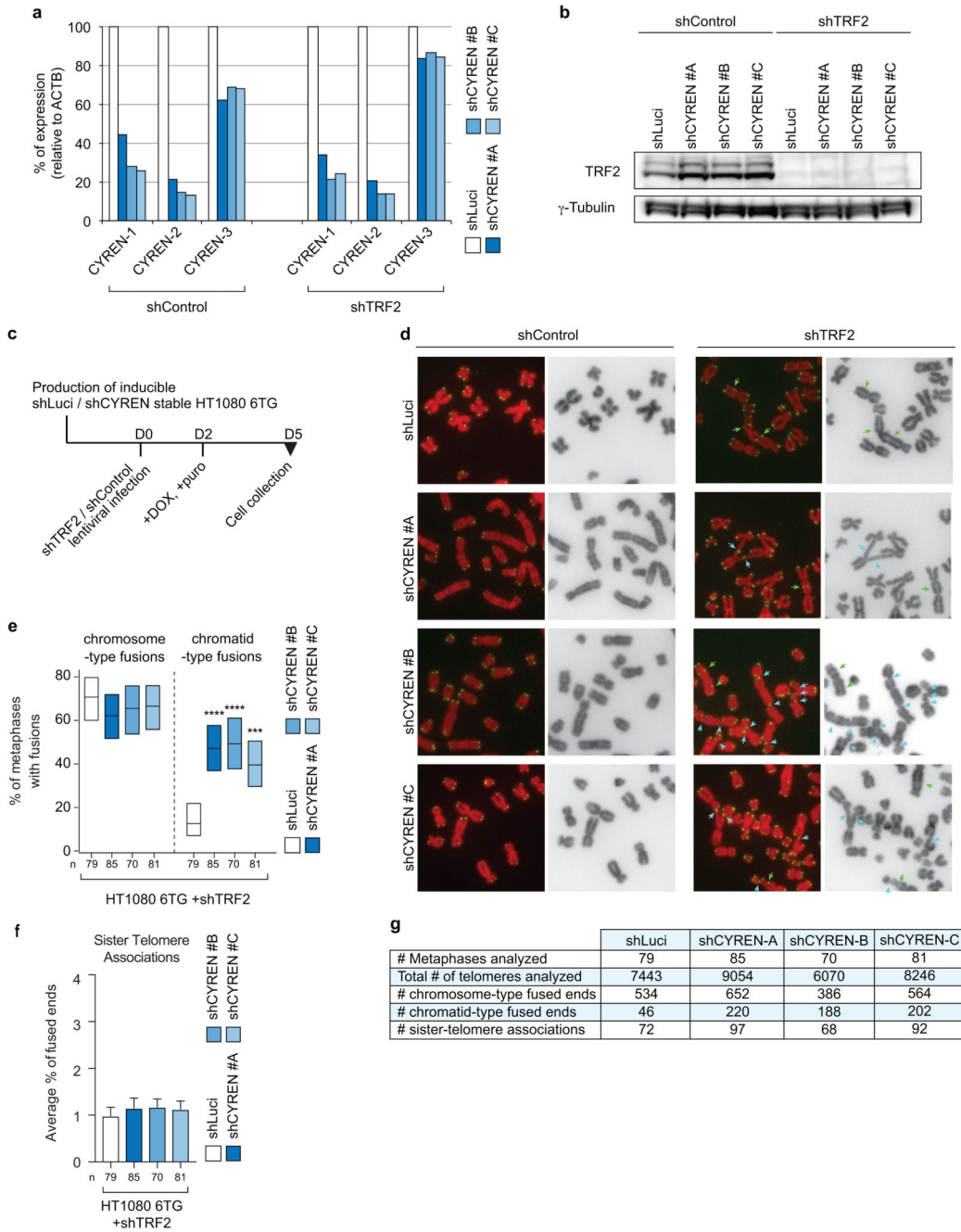
Source Data

All gel source data are available in Supplementary Figure 1.

Data availability statement

All data and reagents are available from the corresponding author (J.K.) upon reasonable request.
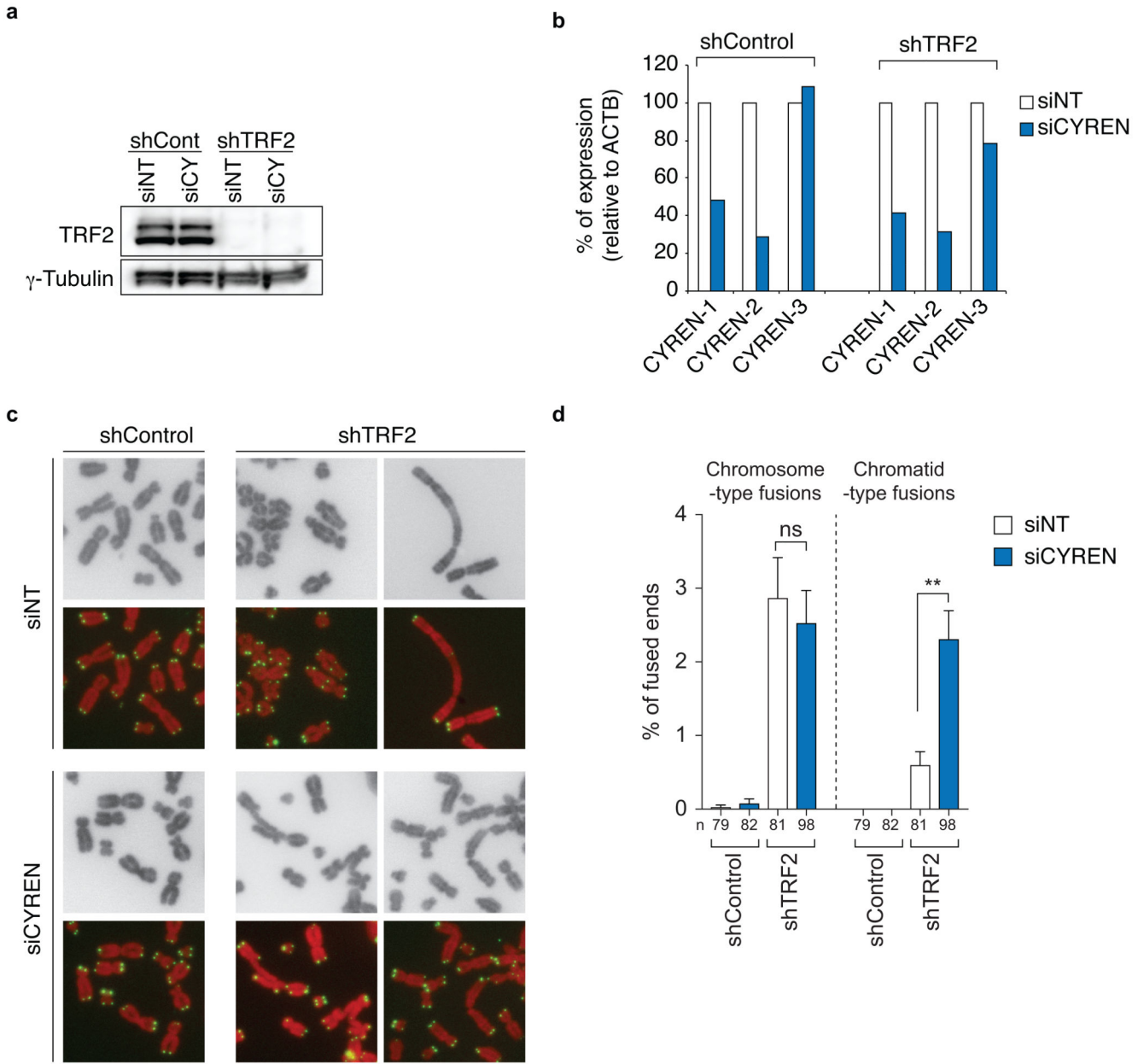
Extended Data

Extended data Figure 1. CYREN depletion leads to chromatid-type fusions at deprotected telomeres.
a, qRT-PCR measurement of CYREN isoforms expression for Figure 1c-e. Normalized to ACTB qRT-PCR. CYREN-1, PCR primers target mRNA transcript variant 1. CYREN-2, PCR primers target mRNA transcript variants 2, 3, 4 and 5. CYREN-3, PCR primers target mRNA transcript variant 7. **b,** Western blot showing TRF2 depletion. For gel source data, see Supplementary Figure 1. **c,** Experimental outline of Figure 1c. HT1080 6TG cells stably

transduced with an inducible control shLuci or three different shCYREN were infected with shControl or shTRF2 on Day 0. shTRF2 transduced cells were selected with puromycin and shCYREN expression was induced with doxycyclin on Day 2. Cells were collected for fusion analysis on Day 5. **d,** Partial metaphase spreads of functional (shControl) and deprotected (shTRF2) telomeres after CYREN depletion. Green arrows: Chromosome-type fusions. Blue arrows: Chromatid-type fusions. **e,** Percentage of cells with fusions ± upper and lower value of 95% confidence intervals, Wilson/Brown test. ****P<0.0001, ***P<0.001. Fisher's exact test, two-sided. n: number of metaphases analysed. **f,** Mean percentage of chromosome ends fused by sister telomere associations. Error bars, s.e.m. ns. One-way ANOVA, Sidak's multiple comparison test. n: number of metaphases analysed. **g,** Number of metaphases analysed, total telomere and fusions counted.

Extended data Figure 2. Chromatid-type fusions induced by CYREN depletion in IMR90 fibroblasts.
a, Western blot showing TRF2 depletion. For gel source data, see Supplementary Figure 1.
b, qRT-PCR measurement of CYREN isoforms expression after siRNA knock-down. Normalized to ACTB qRT-PCR. CYREN-1, PCR primers target mRNA transcript variant 1. CYREN-2, PCR primers target mRNA transcript variants 2, 3, 4 and 5. CYREN-3, PCR primers target mRNA transcript variant 7. **c,** Representative images of partial metaphase spreads of functional (shControl) and deprotected (shTRF2) telomeres after CYREN depletion. **d,** Mean percentage of fused chromosome ends per metaphase. Error bars, s.e.m. ****P<0.01. One-way ANOVA, Sidak's multiple comparison test. n: number of metaphases analysed.
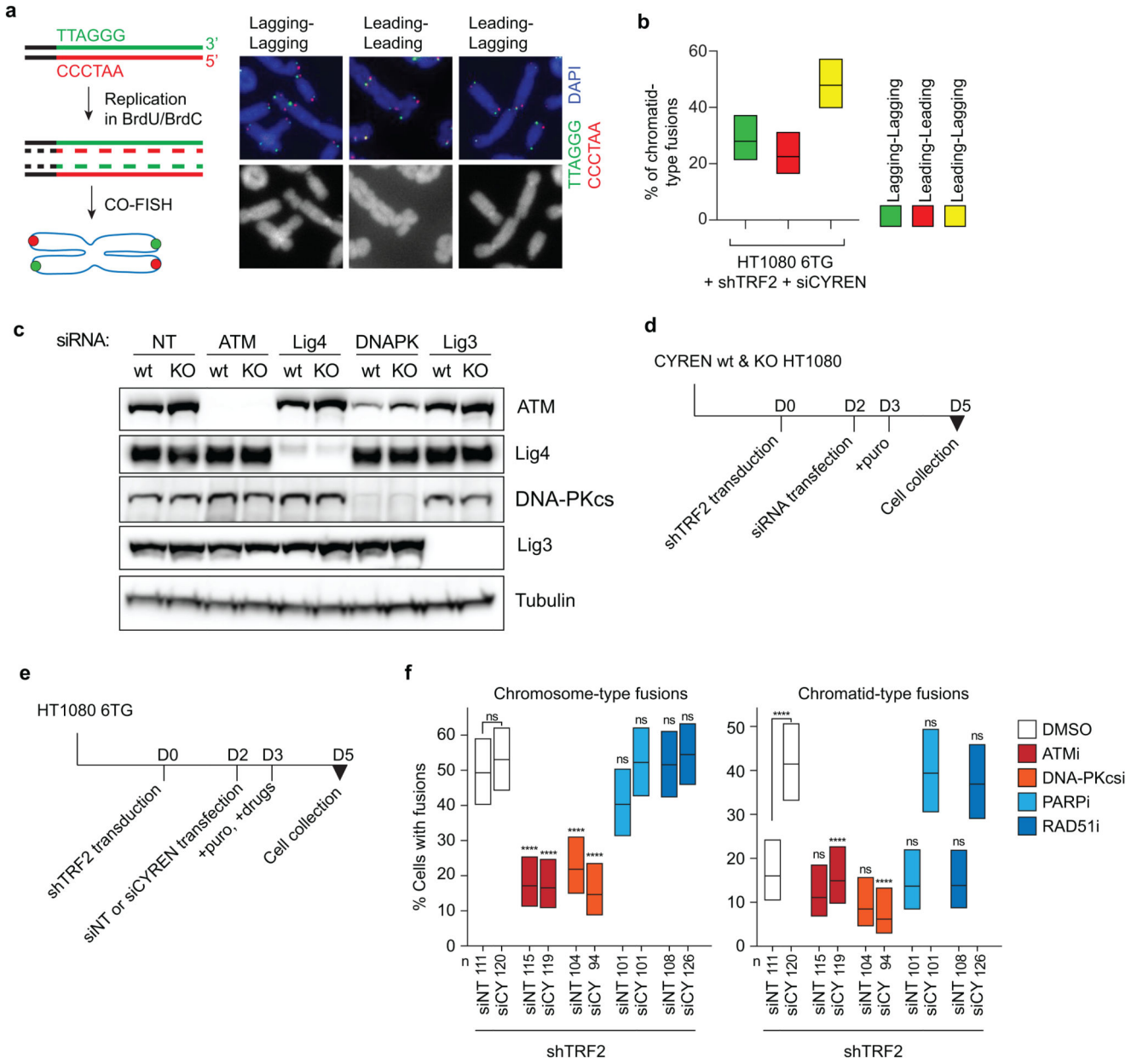
Extended data Figure 3. CYREN prevents cNHEJ in S and G2 at deprotected telomeres.
a, Schematic of CO-FISH. Chromatid-type fusions involving leading and lagging strands. **b,**
Percentage of fusions ± upper and lower value of 95% confidence intervals, Wilson/Brown
test. 126 fusions counted. **c,** Western blot showing knockdown of ATM, Ligase 4, DNA-
PKcs and Ligase 3 in Figure 2c. For gel source data, see Supplementary Figure 1. **d,**
Experimental timeline for Figure 2c. CYREN[wt] and CYREN[KO] HT1080 cells were infected
with shTRF2 on Day 0, followed by transfection with siRNAs on Day 2. On Day 3, shTRF2
infected cells were selected with Puromycin and cells were collected for fusion analysis on
Day 5. **e,** Experimental timeline for Extended data Figure 3d. HT1080 6TG were stably
transduced with shTRF2 on Day 0, followed by transfection with Non-Targetting (NT) or

CYREN siRNAs on Day 2. On Day 3, shTRF2 infected cells were selected with Puromycin and inhibitors were added. Cells were collected for fusion analysis on Day 5. **f,** Percentage of cells with fusions ± upper and lower value of 95% confidence intervals, Wilson/Brown test. Cells were treated for 48 hours with DMSO or the following inhibitors: ATMi (KU-55933) 10μM, DNA-PKcsi (NU-7441) 1μM, PARPi (Olaparib) 10μM, RAD51i (RI-1) 20μM. ****P<0.0001, ns non significant. Fisher's exact test, two-sided. Experiment shown is representative of two biological replicates.
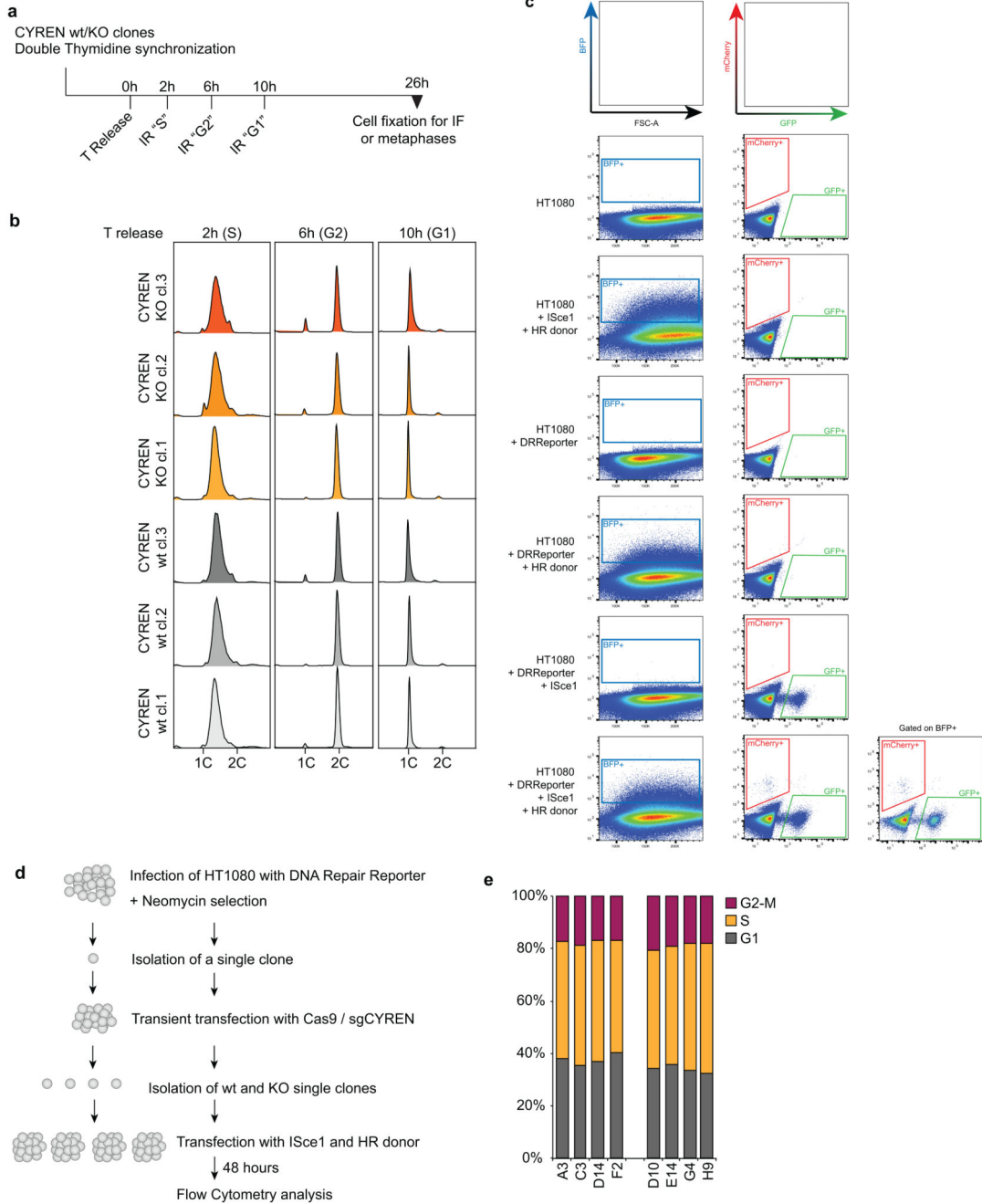
Extended data Figure 4. CYREN regulates the DSB pathway choice at intrachromosomal breaks.

a, Experimental timeline for Figure 3a-b. CYREN^wt and CYREN^KO clonal HT1080 were synchronised by double thymdine block, irradiated at 2 Gray 2 hours, 6 hours and 10 hours after Thymidine release, corresponding to S, G2 and G1 phases of the cell cycle, respectively. Cells were arrested for Immuno-Fluorescence or chromosome spreads 26 hours after thymidine release. **b,** Cell cycle profiles of cells used in Figure 3a-b, 2 hours, 6 hours and 10 hours after Thymidine release. 20,000 cells were analysed. **c,** Representative flow cytometry controls for the DSB Repair Reporter. 1 million cells per sample were analysed. **d,** Experimental outline of Fig. 3d. A single clone of HT1080 transduced with the DSB Repair Reporter was isolated and transfected with Cas9 and sgCYREN. Single clones were isolated and genotype. Selected wt and KO clones were then transfected with ISce1 and the HR donor, followed by flow cytometry analysis 48 hours later. **e,** Cell cycle distribution of the wt and KO clones obtained by flow cytometry of Propidium Iodide and BrdU labeled cells. 20,000 cells were analysed. 80,000 cells were analysed.
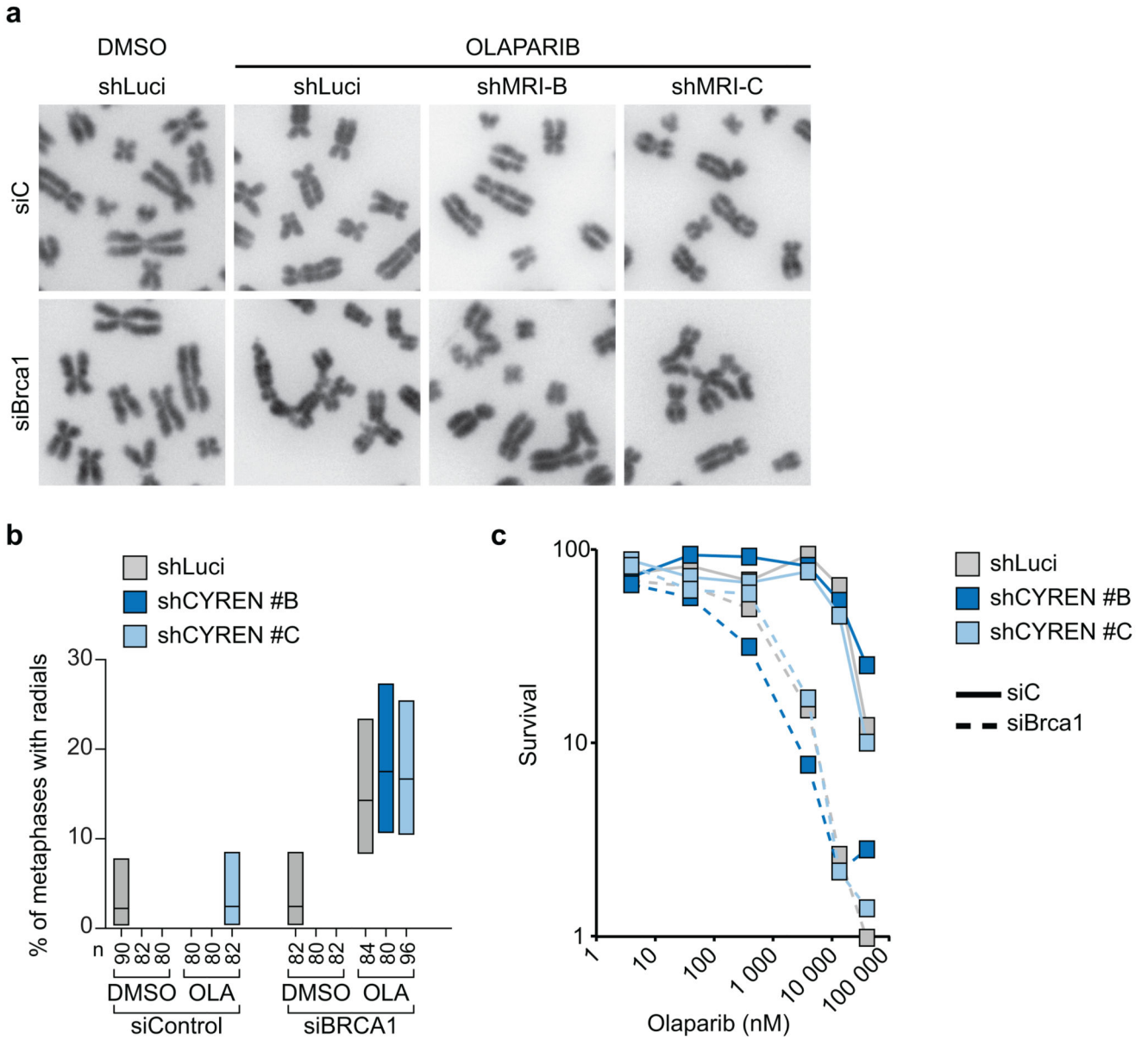
Extended data Figure 5. CYREN does not regulate repair of replication-induced DSBs.
a, Representative images of chromosomes from b. **b.** Percentage of metaphases with radial chromosomes ± upper and lower value of 95% confidence intervals, Wilson/Brown test. n: number of metaphases analysed. Experiment shown is representative of 2 biological replicates. **c,** Percentage of survival to increasing concentrations of PARP inhibitor.

Extended data Figure 6. CYREN isoforms 1 and 2 inhibit cNHEJ.

a, Anti-Flag western blot on whole cell extracts of HT1080 6TG expressing Flag-CYREN isoforms used in Fig. 4b. * indicates two non specific bands. For gel source data, see Supplementary Figure 1. **b,** Experimental outline of Fig. 4b. HT1080 6TG were stably transfected with pcDNA3 empty Flag vector or pcDNA3 expressing CYREN-1-Flag, CYREN-2-Flag or CYREN-3-Flag. Cells were selected and infected with shTRF2 on Day 0, followed by transfection with a control pool of Non-targeting (NT) siRNAs or a pool of siRNAs targeting the 3'UTR of CYREN. shTRF2 infected cells were selected on Day 3 and

cells were collected for fusion analysis on Day 5. **c,** Schematic representation of N-terminal 3FLAG endogenous tagging of CYREN-1 and CYREN-2. **d,** Sequencing of the N-ter 3FLAG-CYREN tagged allele. **e,** Anti-Flag western blot of whole cells extracts from HT1080 and HT1080 with endogenously N-terminally 3xFLAG tagged exon 1 of C7Orf49. Upper band, CYREN-1. Lower band, CYREN-2. Increasing amounts of protein extracts were loaded (5, 10, 15, 20μl). For gel source data, see Supplementary Figure 1. **f,** Schematic representation of C-terminal 3FLAG endogenous tagging of CYREN-1 and CYREN-3. **g,** Sequencing of the C-ter CYREN-3FLAG tagged allele. **h,** FLAG western blot of HT1080 6TG without and with endogenously tagged C-ter CYREN-3FLAG. Increasing amounts of protein extracts were loaded (5, 10, 15, 20μl). For gel source data, see Supplementary Figure 1. **i,** FLAG western blot of 3FLAG-CYREN tagged HT1080 following CYREN knockdown by siRNA. For gel source data, see Supplementary Figure 1.

Extended data Figure 7. CYREN interaction with Ku in S and G2 inhibits cNHEJ.
a, Immunoblotting of a peptide binding array of full length CYREN-1. Each dot represents 20 aa of CYREN-1 with 19 aa overlap with the previous and following peptide. Upper panel, ponceau. Middle panels, duplicate incubation with Ku70/Ku80 recombinant proteins and immunoblotting with anti-Ku70 antibody. Lower panel, control immunoblotting with anti-Ku70 antibody without incubation with recombinant Ku70/80. For gel source data, see Supplementary Figure 1. **b,** Alanine scan of CYREN-1 on residues 9 to 46. FLAG immunoprecipitation of protein extracts from HEK293T cells transfected with pCDNA3.1

plasmids expressing wt CYREN-1-FLAG or each of the single residues mutated to Alanine. Total lysate and FLAG-IP were then immunoblotted with anti FLAG or Ku70 antibodies. For gel source data, see Supplementary Figure 1. **c,** Protein alignment of CYREN-1 Ku Binding Motif among vertebrates. **d,** Photo-crosslinked pull down of a BPA-BIO-CYREN(2-24) peptide in HEK293T protein extract, followed by immunoblotting with anti-Ku70 and Ku80 antibodies. + and ++, 25μM and 50μM of BPA-Bio-CYREN. 100μM of CYREN(2-24) free peptide was used as a competitor. For gel source data, see Supplementary Figure 1. **e,** Experimental outline of Fig. 4d. HT1080 6TG cells stably expressing an inducible control GFP or wt or mutant CYREN-1-3xFlag were transduced with shTRF2 on Day 0 and transfected with a control (NT) pool of siRNAs or a pool of siRNAs targeting the 3'UTR of CYREN on Day 2. Expression of CYREN-1 wt and mutants was induced on Day 3 and cells were collected on Day 5. **f,** FLAG western blot of endogenous C-terminal 3FLAG tagged CYREN-1 and CYREN-2 cells following double thymidine synchronisation. For gel source data, see Supplementary Figure 1.
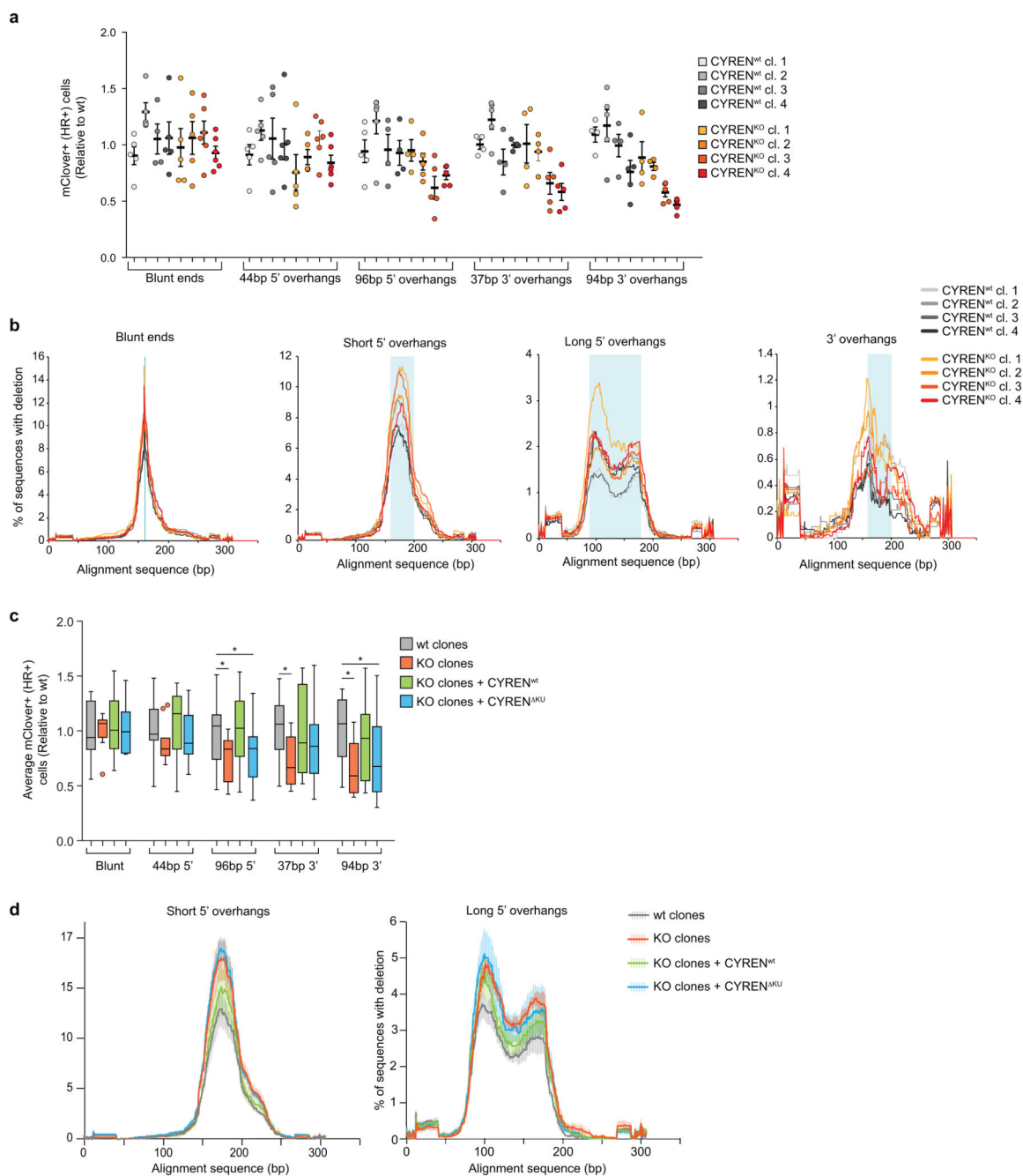
Extended data Figure 8. CYREN inhibits cNHEJ preferentially at breaks with overhangs by preventing processing.

a, Percentage of cells using HR to repair Cas9-induced breaks. Detail of 4 wt and 4 KO clones used in Fig. 5b. **b,** Deletion profiles of repair of Cas9-induced breaks. Detail profiles of 4 wt and 4 KO clones used in Fig. 5c. Blue line in blunt ends: break site. Blue area: overhang region created by the pair of sgRNAs. **c.** Average percentage of mClover+ cells in 4 wt clones, 4 KO clones, 4 KO clones complemented with wt CYREN and 4 KO clones complemented with mutant CYREN (RPW-AAA), in 3 independent experiments,

normalized to wt. Whiskers: Tuckey. *P<0.05. Unpaired T test. In each experiment, 100,000 cells per sample were analysed. **d,** Deletion profiles of repair of Cas9 breaks. Average percentage of deletion in wt, KO clones, and KO clones complemented with wt CYREN or mutant CYREN (RPW-AAA). Error bars, s.e.m.
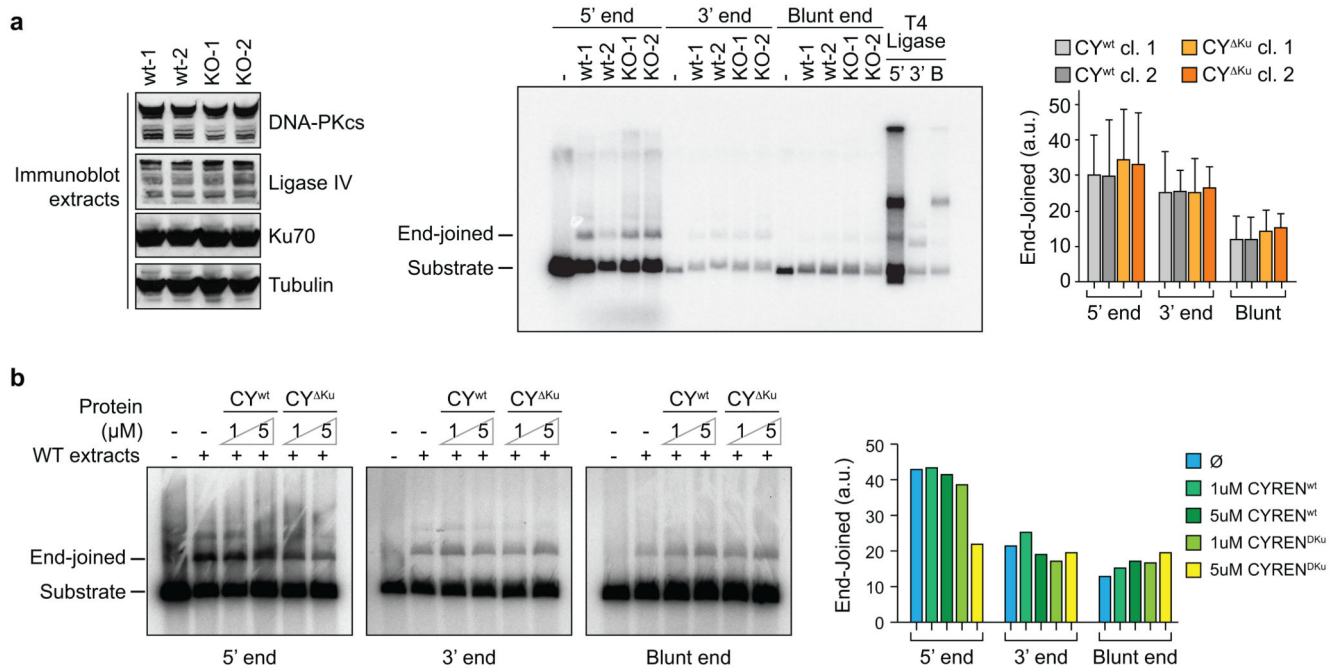
Extended data Figure 9. CYREN does not promote cNHEJ in vitro.
a, In vitro cNHEJ assay using CYREN^{wt} and CYREN^{KO} cells. Left panel: Immunoblots of extracts used in the assay. Middle panel: In Vitro ligation assay. Right panel: quantification. Error bars: standard deviation, 3 independent experiments. For gel source data, see Supplementary Figure 1. **b,** In vitro cNHEJ assay using CYREN^{wt} cells and increasing amounts of recombinant wt CYREN and CYREN ^{Ku} mutant. Right panel: quantification. For gel source data, see Supplementary Figure 1.
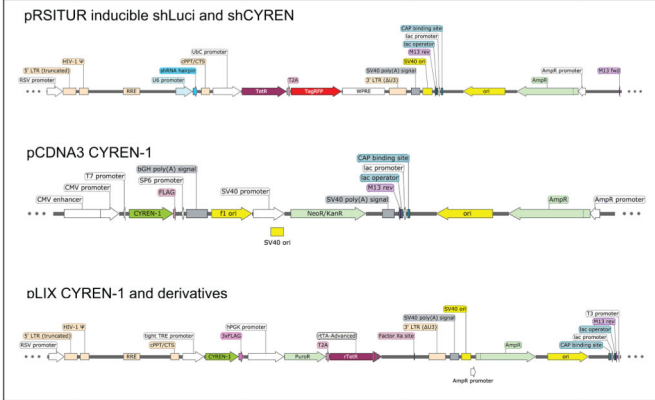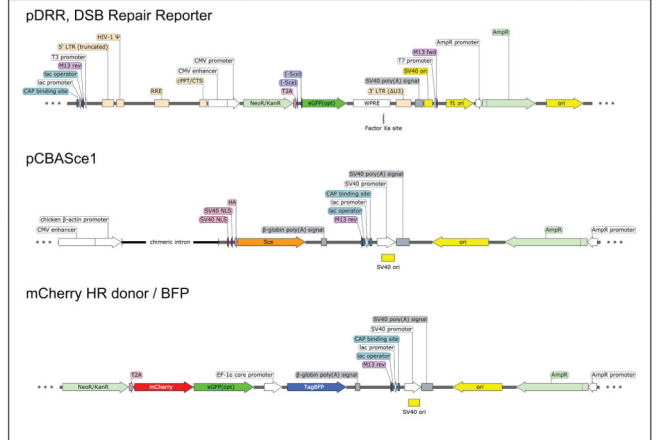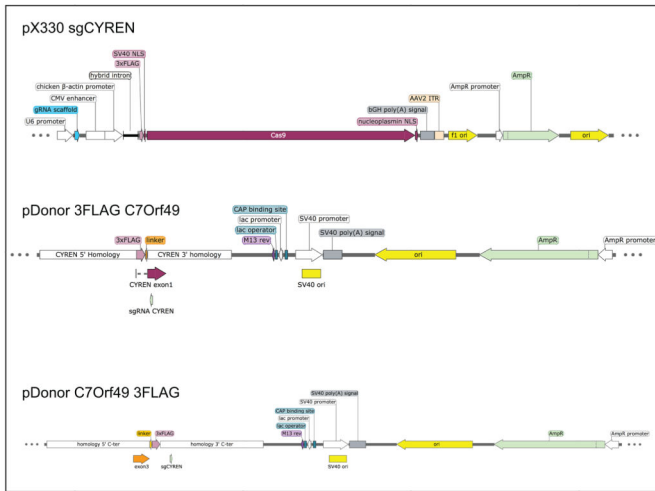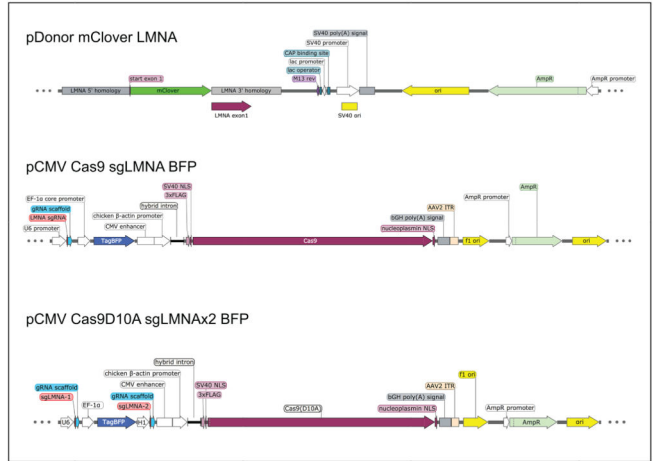
Extended data Figure 10. Maps of plasmids used in Figures 1-2-3-4-5.

Supplementary Material

Refer to Web version on PubMed Central for supplementary material.

Acknowledgements

References

1. Lieber MR. The mechanism of double-strand DNA break repair by the nonhomologous DNA end-joining pathway. Annu Rev Biochem. 2010; 79:181–211. [PubMed: 20192759]

2. Heyer WD, Ehmsen KT, Liu J. Regulation of homologous recombination in eukaryotes. Annu Rev Genet. 2010; 44:113–139. [PubMed: 20690856]

3. Panier S, Boulton SJ. Double-strand break repair: 53BP1 comes into focus. Nat Rev Mol Cell Biol. 2014; 15:7–18. [PubMed: 24326623]

4. Celli GB, de Lange T. DNA processing is not required for ATM-mediated telomere damage response after TRF2 deletion. Nat Cell Biol. 2005; 7:712–718. [PubMed: 15968270]

5. Konishi A, de Lange T. Cell cycle control of telomere protection and NHEJ revealed by a ts mutation in the DNA-binding domain of TRF2. Genes Dev. 2008; 22:1221–1230. [PubMed: 18451109]

6. Escribano-Diaz C, et al. A cell cycle-dependent regulatory circuit composed of 53BP1-RIF1 and BRCA1-CtIP controls DNA repair pathway choice. Mol Cell. 2013; 49:872–883. [PubMed: 23333306]

7. Zimmermann M, Lottersberger F, Buonomo SB, Sfeir A, de Lange T. 53BP1 regulates DSB repair using Rif1 to control 5' end resection. Science. 2013; 339:700–704. [PubMed: 23306437]

8. Chapman JR, Taylor MR, Boulton SJ. Playing the end game: DNA double-strand break repair pathway choice. Mol Cell. 2012; 47:497–510. [PubMed: 22920291]

9. Beucher A, et al. ATM and Artemis promote homologous recombination of radiation-induced DNA double-strand breaks in G2. EMBO J. 2009; 28:3413–3427. [PubMed: 19779458]

10. Symington LS, Gautier J. Double-strand break end resection and repair pathway choice. Annu Rev Genet. 2011; 45:247–271. [PubMed: 21910633]

11. Agarwal S, et al. Isolation, characterization, and genetic complementation of a cellular mutant resistant to retroviral infection. Proc Natl Acad Sci U S A. 2006; 103:15933–15938. [PubMed: 17043244]

12. Slavoff SA, Heo J, Budnik BA, Hanakahi LA, Saghatelian A. A human short open reading frame (sORF)-encoded polypeptide that stimulates DNA end joining. J Biol Chem. 2014; 289:10950–10957. [PubMed: 24610814]

13. van Steensel B, Smogorzewska A, de Lange T. TRF2 protects human telomeres from end-to-end fusions. Cell. 1998; 92:401–413. [PubMed: 9476899]

14. Doksani Y, Wu JY, de Lange T, Zhuang X. Super-resolution fluorescence imaging of telomeres reveals TRF2-dependent T-loop formation. Cell. 2013; 155:345–356. [PubMed: 24120135]

15. Okamoto K, et al. A two-step mechanism for TRF2-mediated chromosome-end protection. Nature. 2013; 494:502–505. [PubMed: 23389450]

16. Karlseder J, Broccoli D, Dai Y, Hardy S, de Lange T. p53- and ATM-dependent apoptosis induced by telomeres lacking TRF2. Science. 1999; 283:1321–1325. [PubMed: 10037601]

17. Smogorzewska A, Karlseder J, Holtgreve-Grez H, Jauch A, de Lange T. DNA ligase IV-dependent NHEJ of deprotected mammalian telomeres in G1 and G2. Curr Biol. 2002; 12:1635–1644. [PubMed: 12361565]

18. Celli GB, Denchi EL, de Lange T. Ku70 stimulates fusion of dysfunctional telomeres yet protects chromosome ends from homologous recombination. Nat Cell Biol. 2006; 8:855–890. [PubMed: 16845383]

19. Sfeir A, Kabir S, van Overbeek M, Celli GB, de Lange T. Loss of Rap1 induces telomere recombination in the absence of NHEJ or a DNA damage signal. Science. 2010; 327:1657–1661. [PubMed: 20339076]

20. Sfeir A, de Lange T. Removal of shelterin reveals the telomere end-protection problem. Science. 2012; 336:593–597. [PubMed: 22556254]

21. Lazzerini Denchi E, Celli G, de Lange T. Hepatocytes with extensive telomere deprotection and fusion remain viable and regenerate liver mass through endoreduplication. Genes Dev. 2006; 20:2648–2653. [PubMed: 17015429]

22. Denchi EL, de Lange T. Protection of telomeres through independent control of ATM and ATR by TRF2 and POT1. Nature. 2007; 448:1068–1071. [PubMed: 17687332]

23. Wu P, van Overbeek M, Rooney S, de Lange T. Apollo contributes to G overhang maintenance and protects leading-end telomeres. Mol Cell. 2010; 39:606–617. [PubMed: 20619712]

24. Lam YC, et al. SNMIB/Apollo protects leading-strand telomeres against NHEJ-mediated repair. EMBO J. 2010; 29:2230–2241. [PubMed: 20551906]

25. Hickson I, et al. Identification and characterization of a novel and specific inhibitor of the ataxia-telangiectasia mutated kinase ATM. Cancer Res. 2004; 64:9152–9159. [PubMed: 15604286]

26. Leahy JJ, et al. Identification of a highly potent and selective DNA-dependent protein kinase (DNA-PK) inhibitor (NU7441) by screening of chromenone libraries. Bioorg Med Chem Lett. 2004; 14:6083–6087. [PubMed: 15546735]

27. Menear KA, et al. 4-[3-(4-cyclopropanecarbonylpiperazine-1-carbonyl)-4-fluorobenzyl]-2H-phthalazin- 1-one: a novel bioavailable inhibitor of poly(ADP-ribose) polymerase-1. J Med Chem. 2008; 51:6581–6591. [PubMed: 18800822]

28. Budke B, et al. RI-1: a chemical inhibitor of RAD51 that disrupts homologous recombination in human cells. Nucleic Acids Res. 2012; 40:7347–7357. [PubMed: 22573178]

29. Grundy GJ, et al. The Ku-binding motif is a conserved module for recruitment and stimulation of non-homologous end-joining proteins. Nat Commun. 2016; 7:11242. [PubMed: 27063109]

30. Shibata A, et al. Factors determining DNA double-strand break repair pathway choice in G2 phase. EMBO J. 2011; 30:1079–1092. [PubMed: 21317870]

31. Le Poole IC, et al. Generation of a human melanocyte cell line by introduction of HPV16 E6 and E7 genes. In Vitro Cell Dev Biol Anim. 1997; 33:42–49. [PubMed: 9028834]

32. Sarbassov DD, Guertin DA, Ali SM, Sabatini DM. Phosphorylation and regulation of Akt/PKB by the rictor-mTOR complex. Science. 2005; 307:1098–1101. [PubMed: 15718470]

33. Cong L, et al. Multiplex genome engineering using CRISPR/Cas systems. Science. 2013; 339

34. Richardson C, Moynahan ME, Jasin M. Double-strand break repair by interchromosomal recombination: suppression of chromosomal translocations. Genes Dev. 1998; 12:3831–3842. [PubMed: 9869637]

35. Campeau E, et al. A versatile viral system for expression and depletion of proteins in mammalian cells. PLoS One. 2009; 4:e6529. [PubMed: 19657394]

36. O'Sullivan RJ, et al. Rapid induction of alternative lengthening of telomeres by depletion of the histone chaperone ASF1. Nat Struct Mol Biol. 2014; 21:167–174. [PubMed: 24413054]

37. O'Sullivan RJ, Kubicek S, Schreiber SL, Karlseder J. Reduced histone biosynthesis and chromatin changes arising from a damage signal at telomeres. Nat Struct Mol Biol. 2010; 17:1218–1225. [PubMed: 20890289]

38. Vannier J-B, Pavicic-Kaltenbrunner V, Petalcorin MIR, Ding H, Boulton SJ. RTEL1 Dismantles T Loops and Counteracts Telomeric G4-DNA to Maintain Telomere Integrity. Cell. 2012; 149:795–806. [PubMed: 22579284]
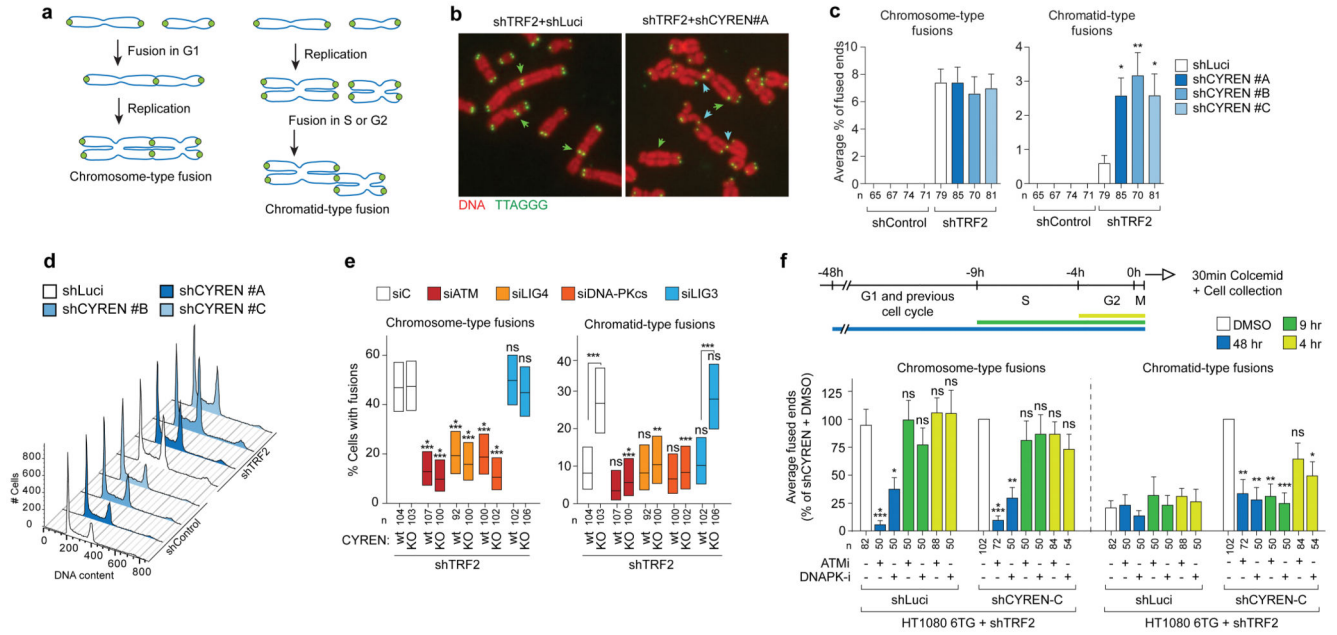
Figure 1. CYREN depletion reactivates cNHEJ in S and G2 at deprotected telomeres.
a, Schematic outcome of telomere fusions. **b,** Partial metaphase spreads of deprotected (shTRF2) telomeres after CYREN depletion. Green arrows: Chromosome-type fusions. Blue arrows: Chromatid-type fusions. **c,** Mean percentage of fused chromosome ends per metaphase, separated in chromosome-type and chromatid-type fusions. Error bars, s.e.m. **P<0.01, *P<0.05. One-way ANOVA, Sidak's multiple comparison test. n: number of metaphases analysed. Experiment shown is representative of two biological replicates. **d,** Cell cycle profiles of cells from c. 12,000 cells were analysed. **e,** Percentage of cells with fusions ± upper and lower value of 95% confidence intervals, Wilson/Brown test. ****P<0.0001, ***P<0.001, **P<0.01. Fisher's exact test, two-sided. n: number of metaphases analysed. **f,** Upper panel, experimental outline. Lower panel, mean percentage of fused ends per metaphase. Error bars, s.e.m. ***P<0.001, **P<0.01, *P<0.05. One-way ANOVA. Sidak's multiple comparison test. n: number of metaphases analysed. Experiment shown is representative of two biological replicates.
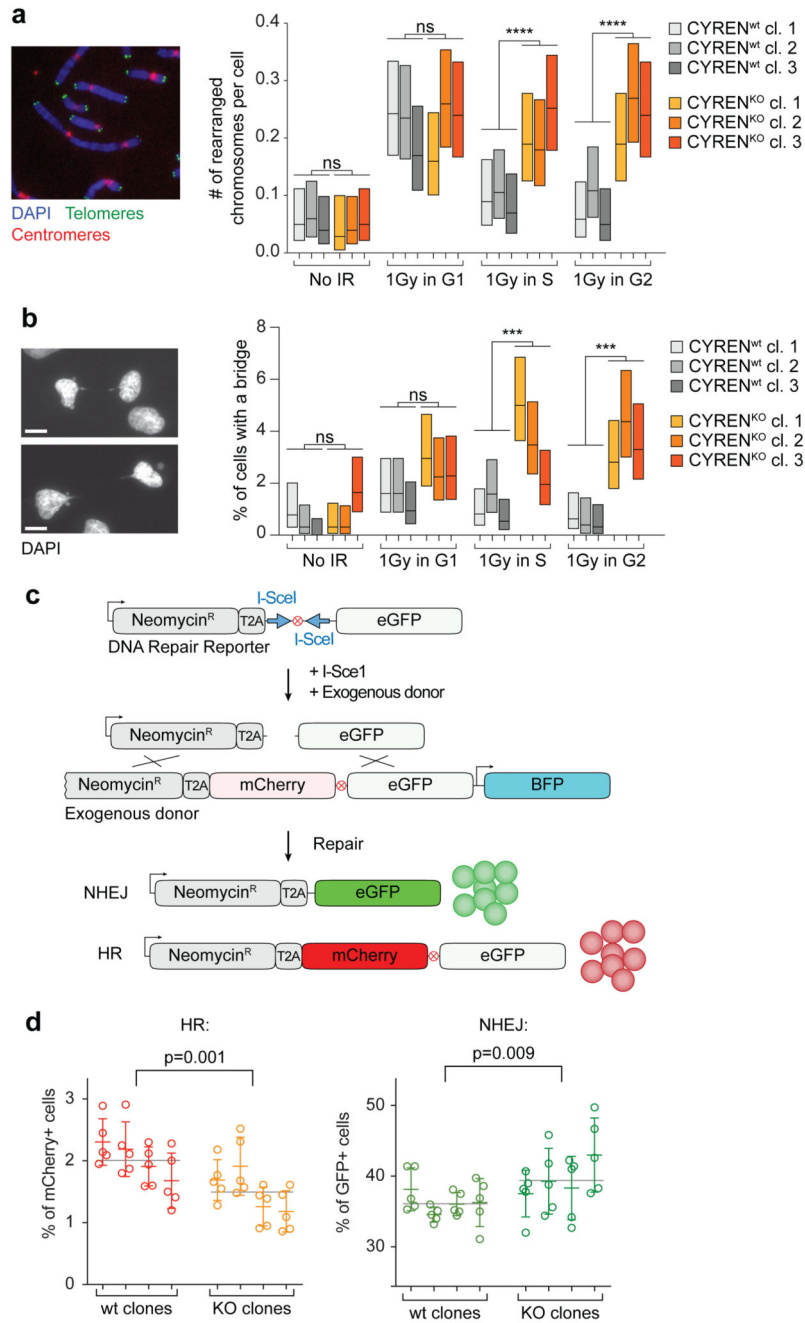
Figure 2. CYREN inhibits NHEJ at intrachromosomal breaks.
a, Average number of rearranged chromosomes per cell ± upper and lower value of 95% confidence intervals, Wilson/Brown test. ****P<0.0001. Two-tailed unpaired t-test. 120 metaphases analysed per condition in 3 biological replicates. **b,** Percentage of cells with a bridge ± upper and lower value of 95% confidence intervals, Wilson/Brown test. ***P<0.001. Two-tailed unpaired t-test. 300 cells analysed in 3 biological replicates. **c, d,** Percentage of GFP+ and mCherry+ cells, gated on BFP+, of five biological replicates. Mean

± s.d. is indicated. Gray line, mean of all wt or KO clones. P values, unpaired T test between wt and KO clones. In each experiment, 1 million cells per sample were analysed.
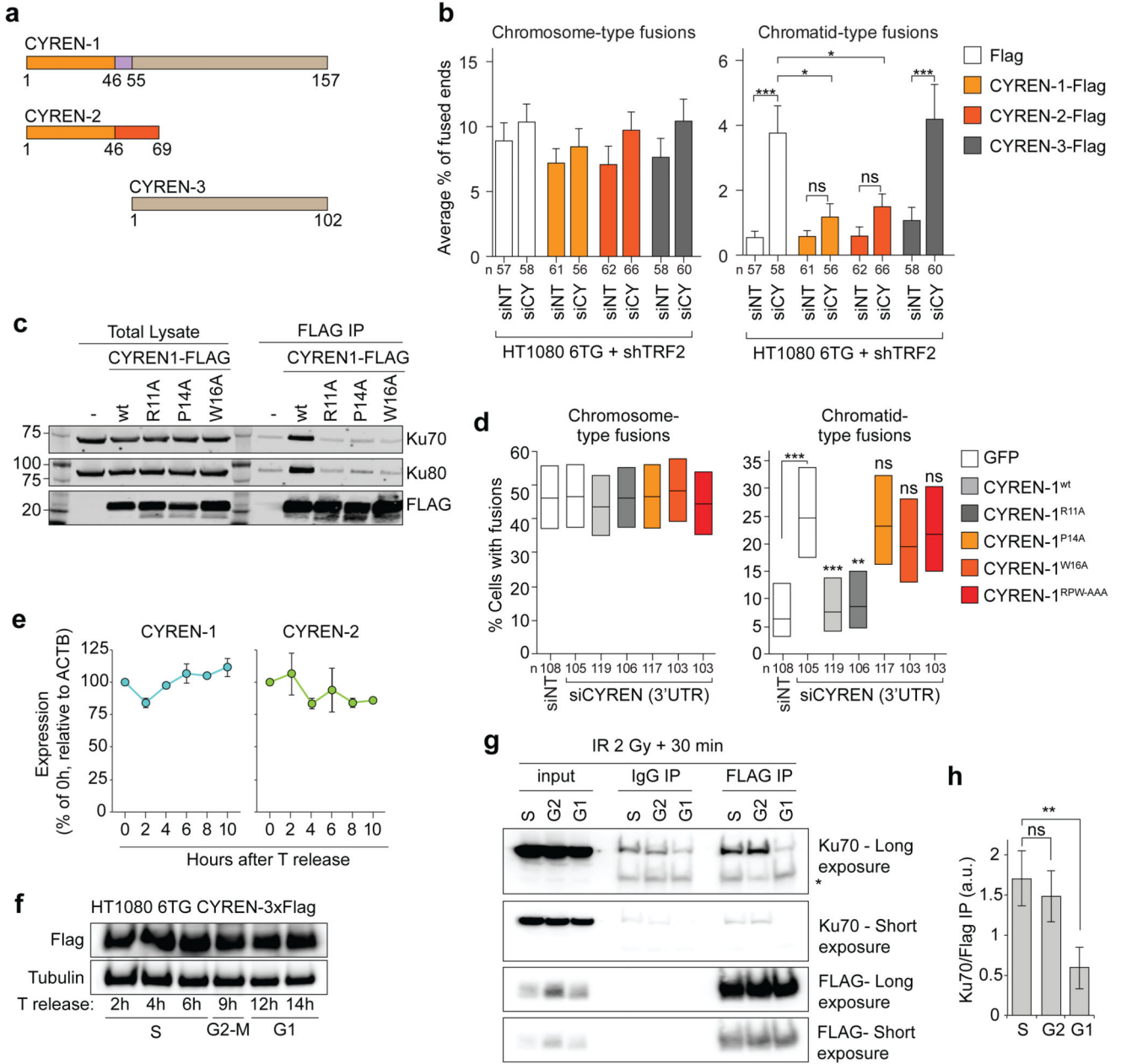
Figure 3. CYREN interaction with Ku in S and G2 inhibits cNHEJ.
a, CYREN isoforms. **b,** Mean percentage of fused ends per metaphase. Error bars, s.e.m.
***P<0.001, *P<0.05, ns non significant. One-way ANOVA, Sidak's multiple comparison
test. n: number of metaphases analysed. Experiment shown is representative of two
biological replicates. **c,** Co-Immunoprecipitation of CYREN-1-3FLAG with Ku70/80 in
HEK293T. For gel source data see Supplementary Figure 1. **d,** Percentage of fusions ± upper
and lower value of 95% confidence intervals, Wilson/Brown test. ***P<0.001, **P<0.01, ns
non significant. Fisher's exact test, two-sided. **e,** Relative abundance of CYREN-1 and 2
mRNA in double Thymidine synchronized cells. **f,** Immunoblotting of 3FLAG-CYREN-1 in

double Thymidine synchronized cells. **g.** FLAG immunoprecipitation of CYREN1-3FLAG with 2 Gy irradiation followed by FLAG and Ku70 immunoblotting in double Thymidine synchronized cells. *unspecific band. For gel source data see Supplementary Figure 1. Experiment shown is representative of 4 biological replicates. **h,** Quantification of g. Error bars, s.e.m. over 4 independent experiments. **P<0.01. Ordinary one-way ANOVA.

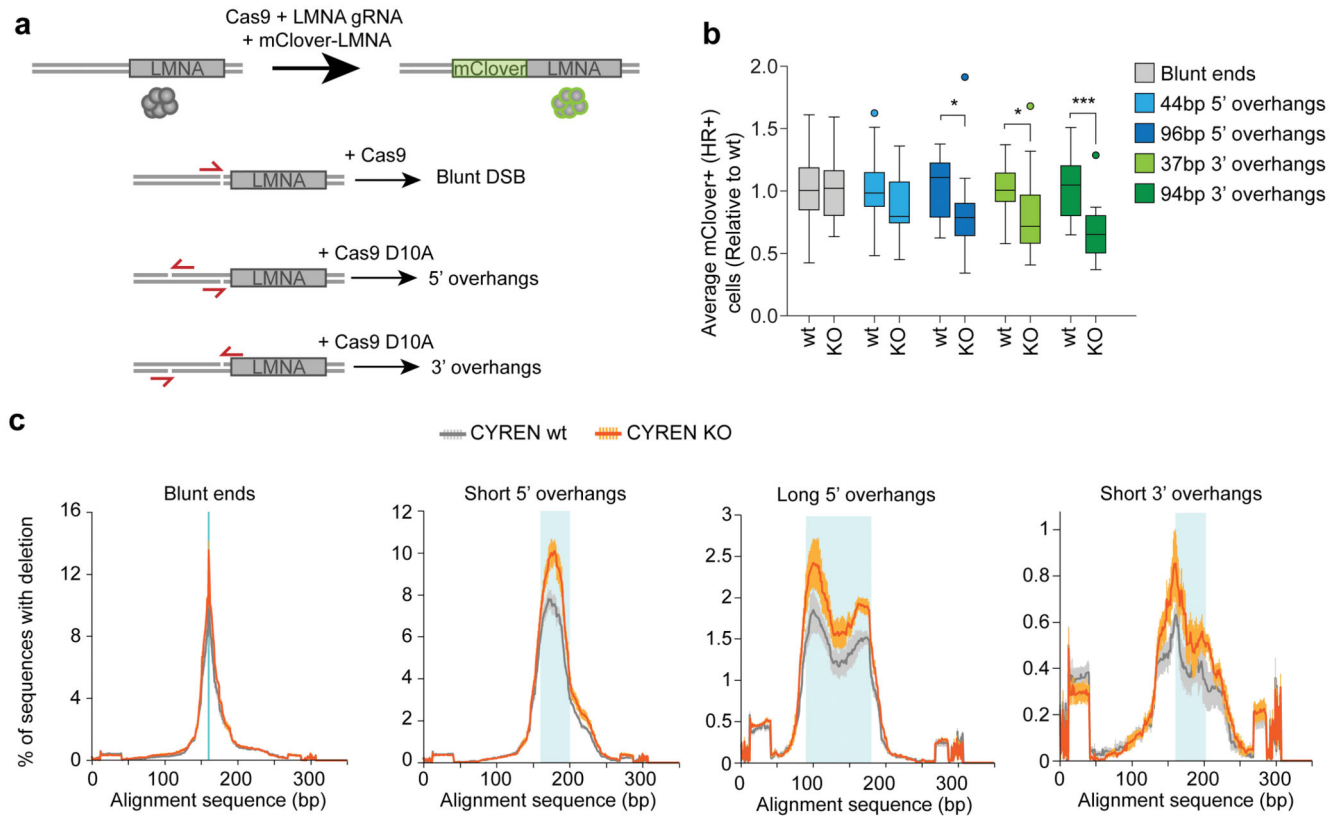**Figure 4. CYREN prevents overhang processing.**
a, LMNA Cas9 reporter. CRISPR/Cas9 and sgRNAs target the 5' UTR of LMNA. HR fuses mClover to LMNA for repair. Cas9 with sgRNAs (red arrows) generate different breaks. **b,** Average percentage of mClover+ cells in 4 wt and 4 KO clones in 5 independent experiments, normalized to wt. Whiskers: Tuckey. ***P<0.001, *P<0.05. Ordinary one-way ANOVA. In each experiment, 250,000 cells per sample were analysed. **c,** Deletion profiles of repair of Cas9 breaks. Average percentage of deletion in 4 wt and 4 KO clones. Error bars, s.e.m. Blue line in blunt ends: break site. Blue area: overhang region created by the pair of sgRNAs.